Applied Physics Letters

Coupling of magnetic field and lattice strain and its impact on electronic phase separation in $La_{0.335}Pr_{0.335}Ca_{0.33}MnO_3$/ ferroelectric crystal heterostructures

Cite as: Appl. Phys. Lett. **103**, 263507 (2013); https://doi.org/10.1063/1.4860415
Submitted: 14 November 2013 . Accepted: 06 December 2013 . Published Online: 31 December 2013

M. Zheng, X. Y. Li, M. M. Yang, Q. X. Zhu, Y. Wang, X. M. Li, X. Shi, H. L. W. Chan, X. G. Li, H. S. Luo, and R. K. Zheng

Coupling of magnetic field and lattice strain and its impact on electronic phase separation in $La_{0.335}Pr_{0.335}Ca_{0.33}MnO_3$/ferroelectric crystal heterostructures

M. Zheng,[1] X. Y. Li,[1,2] M. M. Yang,[1] Q. X. Zhu,[1] Y. Wang,[3] X. M. Li,[1] X. Shi,[1] H. L. W. Chan,[3] X. G. Li,[4] H. S. Luo,[1] and R. K. Zheng[1,a)]
[1]*State Key Laboratory of High Performance Ceramics and Superfine Microstructure, Shanghai Institute of Ceramics, Chinese Academy of Sciences, Shanghai 200050, China*
[2]*Department of Materials Science and Engineering, Nanjing University of Science and Technology, Nanjing 210094, China*
[3]*Department of Applied Physics and Materials Research Center, The Hong Kong Polytechnic University, Hong Kong, China*
[4]*Hefei National Laboratory for Physical Sciences at Microscale and Department of Physics, University of Science and Technology of China, Hefei 230026, China*

(Received 14 November 2013; accepted 6 December 2013; published online 31 December 2013)

Phase-separated $La_{0.335}Pr_{0.335}Ca_{0.33}MnO_3$ films were epitaxially grown on (001)- and (111)-oriented ferroelectric single-crystal substrates. Upon poling along the [001] or [111] direction, dramatic decrease in resistance, up to 99.98%, and complete melting of the charge-ordered phase were observed, caused by poling-induced strain rather than accumulation of electrostatic charge at interface. Such poling-induced strain effects can be effectively tuned by a magnetic field and mediated by electronic phase separation. In particular, our findings show that the evolution of the strength of electronic phase separation against temperature and magnetic field can be determined by measuring the strain-tunability of resistance $[(\Delta R/R)_{strain}]$ under magnetic fields. © *2013 AIP Publishing LLC*. [http://dx.doi.org/10.1063/1.4860415]

Many exotic phenomena such as colossal magnetoresistance effect, metal-insulator transition, and high temperature superconductivity, in complex oxides, are deeply associated with the emergence of microscopic electronic phase separation (EPS). Perovskite manganite of $La_{1-x-y}Pr_yCa_xMnO_3$ is one of the well-known systems that displays large scale EPS into ferromagnetic metallic (FMM) phase and charge-ordered antiferromagnetic insulating (CO/AFI) phase at low temperatures.[1–18] Although EPS in manganites has been widely studied over the past decade, issues regarding EPS, such as the length scale of the FMM phase, the mechanism that causes EPS, and the effects of in-plane strain on EPS, have remained controversial so far due to inconsistent experimental findings. For example, Gillaspie *et al.*[9] and Wu *et al.*[10] found that the in-plane tensile strain stabilizes the CO/AFI phase but disfavors FMM phase for $La_{0.325}Pr_{0.3}Ca_{0.375}MnO_3$ films epitaxially grown on $SrTiO_3$ and $LaAlO_3$ substrates, respectively, while Jeen and Biswas,[11] and Ward *et al.*[2] reported that the in-plane tensile strain destabilizes the CO/AFI phase but favors FMM phase for $La_{0.268}Pr_{0.402}Ca_{0.33}MnO_3$ and $La_{0.325}Pr_{0.3}Ca_{0.375}MnO_3$ films on $NdGaO_3$ and $SrLaGaO_4$ substrates. Besides substrate-induced strain, quenched disorders,[12,13] local Jahn-Teller type lattice distortion,[14] oxygen content,[10] intragranular strain[15] and dead layer at interface,[16] etc, are reported to have a strong influence over the EPS, making it rather difficult to obtain the intrinsic effects of lattice strain on EPS. To rule out the effects of these extrinsic variables on EPS, Dekker *et al.*,[17] Zhang *et al.*,[18] Wang *et al.*,[19] and Chen *et al.*[20] *in situ* applied in-plane compressive strain to $La_{1-x-y}Pr_yCa_xMnO_3$ films grown on $(1-x)Pb(Mg_{1/3}Nb_{1/2})O_3$-$xPbTiO_3$ ferroelectric substrates, using the piezoelectric strain and found that the in-plane compressive strain favors the FMM phase. In spite of all these efforts, certain important questions concerning EPS remain unanswered, for example, the way the relative strength of EPS evolves with strain and magnetic field, and how lattice strain interacts with magnetic field for $La_{1-x-y}Pr_yCa_xMnO_3$ films.

In this work, we used polished (001)-oriented $0.67Pb(Mg_{1/3}Nb_{1/2})O_3$-$0.33PbTiO_3$ (PMN-PT) and (111)-oriented $0.31Pb(In_{1/2}Nb_{1/2})O_3$-$0.35Pb(Mg_{1/3}Nb_{1/2})O_3$-$0.34PbTiO_3$ (PIN-PMN-PT) single-crystal substrates to grow phase-separated $(La_{1-x}Pr_x)_{0.67}Ca_{0.33}MnO_3$ $(x = 0.5)$ (LPCMO) films and *in situ* manipulated the in-plane strain of LPCMO films by poling the ferroelectric substrates along the [001] and [111] directions, respectively. Our study focuses on examining how the relative strength of EPS evolves with magnetic field and the mutual interactions between lattice strain and magnetic field.

PMN-PT and PIN-PMN-PT single crystals were cut into (001)- and (111)-oriented rectangular plates and polished to a root-mean-square roughness $R_q < 1$ nm. Such polished PMN-PT(001) substrates show a well-defined polarization-electric field hysteresis loop, a butterfly strain-electric field loop [Figs. 1(e) and 1(f)] and a piezoelectric coefficient ($d_{33} \sim 1650$ pC/N). In contrast, PIN-PMN-PT(111) substrates show weak ferroelectricity [Fig. 1(e)] and piezoelectricity ($d_{33} \sim 100$ pC/N) with a relatively small electric-field-induced strain [Fig. 1(f)], since they hold a tetragonal structure.[21]

LPCMO films were deposited on polished substrates by pulsed laser deposition. The thickness of the films is ~34 nm, as can be seen from the cross-sectional back-scattered electron (BSE) image in Fig. 1(g). All films show smooth surface with $R_q \sim 1$ nm. A selected atomic force

a)E-mail: zrk@ustc.edu

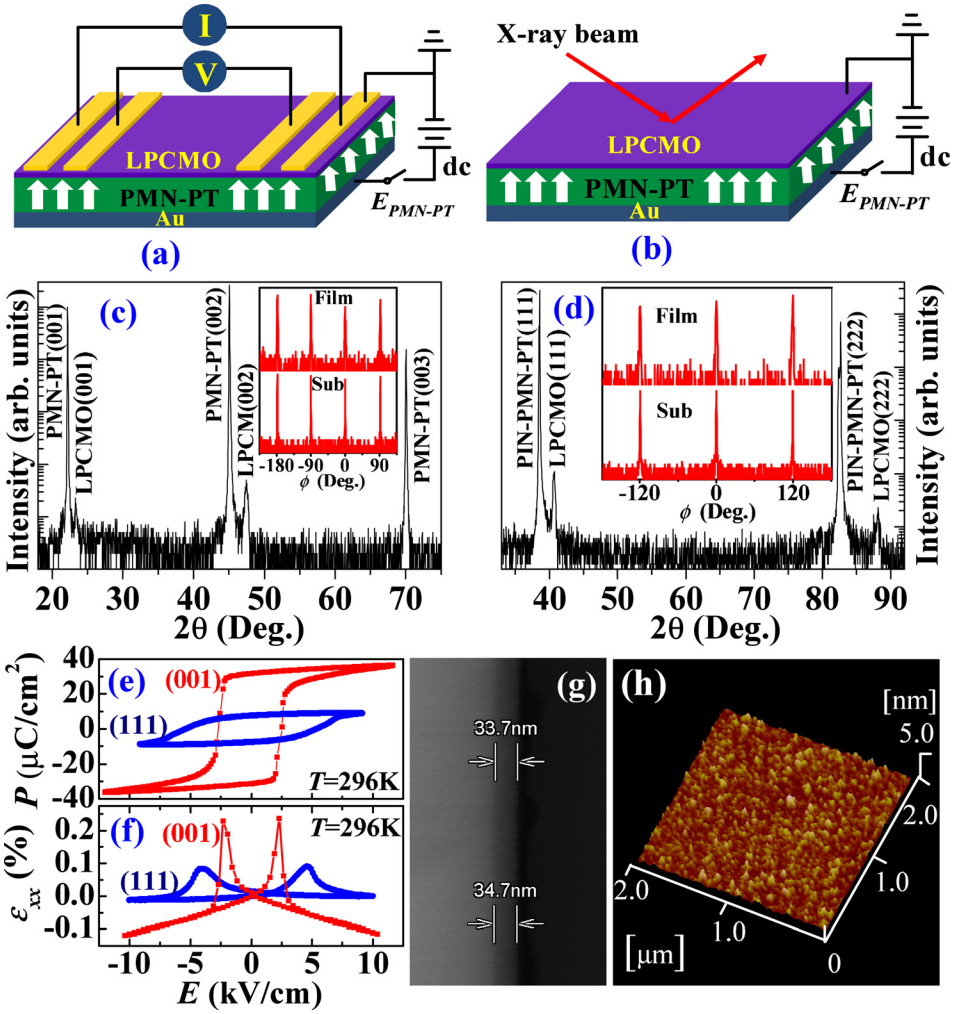

FIG. 1. (a) and (b) Schematic of the experimental setups for *in situ* measurements of film resistance and strain, respectively. (c) and (d) XRD θ-2θ scans of the LPCMO films. Insets: XRD ϕ scans of the films and substrates. (e) and (f) Polarization and in-plane strain versus E for the PMN-PT(001) (red) and PIN-PMN-PT(111) (blue) substrates. (g) and (h) Cross-sectional BSE image and surface morphology of the LPCMO(111) film, respectively.

microscopy image taken on a LPCMO(111) film was shown in Fig. 1(h). X-ray diffraction (XRD) data were collected using a Bruker D8 Discover X-ray diffractometer, equipped with Cu $K_{\alpha 1}$ radiation ($K_{\alpha 1} = 1.5406$ Å). Figs. 1(a) and 1(b) show the schematic of the experimental setups for *in situ* measurements of resistance and strain of LPCMO films, respectively. Electric-field-induced in-plane strain in substrates was measured using a strain gauge that was attached to the substrate surface with epoxy. Poling and polarization switching was achieved by applying dc electric fields across the substrates using the LPCMO film and sputtered Au film as top and bottom electrodes, respectively. The film resistance was measured using a physical property measurement system (PPMS-9, Quantum Design). Magnetic data were collected using a SQUID magnetometer (MPMS XL-5, Quantum Design).

Figures 1(c) and 1(d) show the XRD θ-2θ scans for the LPCMO films grown on the PMN-PT(001) and PIN-PMN-PT(111) substrates, respectively. Apparently, strong (00l) and (lll) ($l = 1$, 2) diffraction peaks could be seen from the LPCMO(001) and LPCMO(111) films, respectively, suggesting both LPCMO films are of single phase and are highly (001)- and (111)-oriented. XRD ϕ scans taken on the LPCMO (101) diffraction peaks show that fourfold (trifold) symmetrical diffraction peaks appear every 90° (120°) degree, a clear sign of "cube-on-cube" epitaxial growth of the LPCMO films on the substrates.

The dynamical strain-tuning of the electronic transport property is shown in Fig. 2, where the electric-field-induced relative resistance change $\Delta R/R$ follows the electric-field-induced in-plane compressive strain ($\varepsilon_{xx(Substrate)}$) in the PMN-PT and PIN-PMN-PT substrates effectively. The nonlinear sharp drop in the resistance near E_C of the substrates reveals a strong correlation between electronic transport and $\varepsilon_{xx(Substrate)}$. The induced $\varepsilon_{xx(Substrate)}$, whether perpendicular to the [001] or [111] direction, is effectively transferred to the LPCMO film,

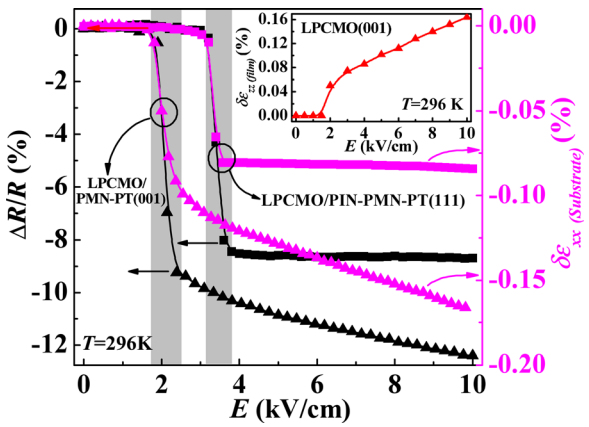

FIG. 2. $\Delta R/R$ of the films and electric-field-induced in-plane strain of the substrates as a function of E. Inset shows the electric-field-induced out-of-plane strain ($\delta\varepsilon_{zz}$) for the LPCMO(001) film.

causing a reduction in the in-plane tensile strain and an increase in the out-of-plane strain of the LPCMO film. *In situ* XRD measurements, indeed, showed that the out-of-plane lattice constant c of the LPCMO(001) film shows a remarkable nonlinear increase near E_C of the PMN-PT(001) substrate (inset of Fig. 2). For $E = 10$ kV/cm, the relative change in c, $\Delta c/c$, defined as $\Delta c/c = [c(E) - c(0)]/c(0)$, for the LPCMO(001) film and the PMN-PT(001) substrate is ~0.164% and ~0.232%, respectively. Such disparity in $\Delta c/c$ could probably be attributed to the different Poisson's ratio of the two materials. The effective strain transferring coefficient α ($\alpha = [(\Delta c/c)_{film}]/[(\Delta c/c)_{PMN-PT}]$) is ~70.7%. Assuming the Poisson's ratio $\nu \sim 0.35$ for the LPCMO film, the electric-field-induced in-plane strain $\Delta a/a$ is estimated to be $\sim -0.152\%$ at $E = 10$ kV/cm, using the equation $(\Delta c/c)_{film} = -2\nu/(1-\nu)(\Delta a/a)_{film}$. The room-temperature resistance-strain coefficient β, $\beta = [(\Delta R/R)_{film}]/[(\Delta a/a)_{film}]$, is ~81.6 at $E = 10$ kV/cm for the LPCMO(001) film. For the LPCMO(001) film, $\Delta R/R$ decreases gradually and linearly with increasing E from ~3.5 to 10 kV/cm, a typical behavior of the resistance change due to the converse-piezoelectric-effect-induced linear decrease in the in-plane tensile strain of the film.[22] A closer look at the variation of $\Delta R/R$ with E for the LPCMO(111) film reveals that $\Delta R/R$ for $E \geq 4$ kV/cm also decreases linearly with the slope of $\Delta R/R$ versus E curve, much smaller than that of the LPCMO(001) film. This finding is consistent with the fact that d_{33} (~100 pC/N) of the PIN-PMN-PT(111) substrate is much smaller than that of the PMN-PT(001) substrate.

Figs. 3(a) and 3(b) show the temperature dependence of the resistance under magnetic fields for the LPCMO(001) film when the PMN-PT(001) substrate was in the unpoled P_r^0 and the positively poled P_r^+ states, respectively. Here, P_r^+ is defined as electric dipole moments pointing to the LPCMO film [see Fig. 1(a)]. For the P_r^0 state and $H = 0$ T, the LPCMO film undergoes a charge-ordering phase transition with decreasing temperature, whose transition temperature

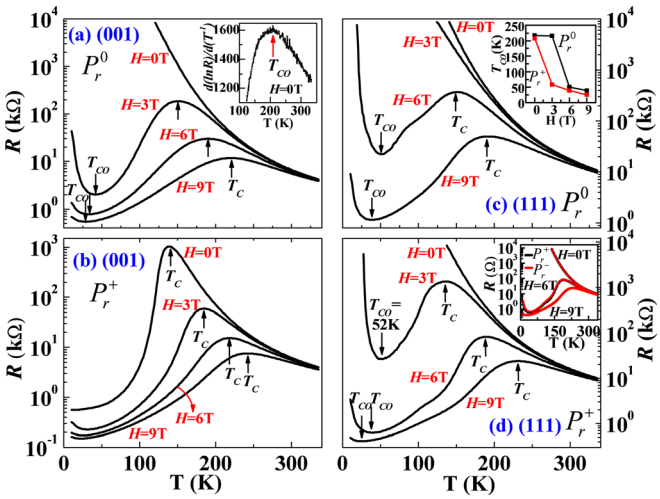

FIG. 3. Temperature dependence of the resistance for the LPCMO films under $H = 0$, 3, 6, and 9 T when the substrates were in the P_r^0 ((a) and (c)) and P_r^+ ((b) and (d)) states, respectively. Inset in (a) shows the $d(\ln R)/d(T^{-1}) - T$ curve. Inset in (c) shows T_{CO} versus H curve for the P_r^0 and P_r^+ states, respectively. Inset in (d) shows temperature dependence of resistance for the LPCMO(111) film under $H = 0$, 6, and 9 T when the PIN-PMN-PT(111) substrate was in the P_r^+ and P_r^- states, respectively.

T_{CO} (~210 K) can be derived from the $d(\ln R)/d(T^{-1}) - T$ curve[23] shown in the inset of Fig. 3(a). With increasing H to 3 T, the CO/AFI phase was largely converted into the FMM phase, manifested by the magnetic-field-induced insulator-to-metal transition at $T = 150$ K and the dramatic suppression of T_{CO} from 210 K for $H = 0$ T to 41 K for $H = 3$ T. As H increased further, the resistance and T_{CO} were further reduced. For $H = 9$ T, the CO/AFI phase was almost completely melted, since the film is essentially metallic down to 10 K. It is interesting to note that once the PMN-PT(001) substrate was poled positively along the [001] direction with a *dc* field of 10 kV/cm at room temperature, the CO/AFI phase was completely melted even without the application of a magnetic field, as manifested by a strain-induced well-defined insulator-to-metal phase transition at $T = 140$ K [see Fig. 3(b)]. At $T = 10$ K, it is roughly estimated that the resistance was reduced by more than four orders of magnitude. The observation of such a significant ferroelectric poling-induced decrease in resistance and melting of the CO state is believed to be unprecedented[17–20,22] and demonstrates the effectiveness of dynamical strain-manipulation of EPS.

The strong ferroelectric poling-induced effects were also found in the LPCMO(111) film, as can be seen in Figs. 3(c) and 3(d). However, in contrast to that observed in the LPCMO(001) film, the poling-induced strain alone is insufficient to melt the CO/AFI phase of the LPCMO(111) film, as reflected by the insulating nature of the resistance at low temperatures for $H = 0$ T. This could be a result of the relatively small induced strain in the PIN-PMN-PT substrate. From the inset of Fig. 3(c), one can see that T_{CO} for the LPCMO(111) film is most sensitive to the induced strain at $H = 3$ T, where ΔT_{CO} (~158 K) shows the maximum, here $\Delta T_{CO} = T_{CO}(P_r^0) - T_{CO}(P_r^+)$. Obviously, the effects of induced strain on T_{CO} are strongly dependent of the magnetic field. This magnetic-field dependent strain effect is, in fact, closely related to EPS and will be discussed later. Here, we note that similar strong poling-induced strain effects on EPS were also observed in the $(La_{1-x}Pr_x)_{0.67}Ca_{0.33}MnO_3$ ($x = 0.25$) film grown on the PIN-PMN-PT(111) substrate (see Fig. S1 of the supplementary material[24]). Another noteworthy feature is that, regardless of whether the LPCMO(111) film is under $H = 0$, 6, or 9 T, the resistance for the P_r^+ state is similar to that for the P_r^- state, throughout the entire temperature range [see inset of Fig. 3(d)]. Here, P_r^- is defined as electric dipole moments pointing to the bottom gold electrode. This suggests that the ferroelectric (180°) domain switching-induced electrostatic charge at interface has little effects on the electronic transport properties for the LPCMO/PIN-PMN-PT(001) structure, where the strain state rather than polarity determines the change in resistance.

The quantitative effects of poling-induced strain on the resistance for the LPCMO(001) and LPCMO(111) films are presented in Figs. 4(a) and 4(b), respectively, with the strain-tunability of resistance, $(\Delta R/R)_{strain}$, plotted against temperature. Here, $(\Delta R/R)_{strain}$ is defined as $(\Delta R/R)_{strain} = [R(P_r^0) - R(P_r^+)]/R(P_r^0)$. Upon decreasing temperature, $(\Delta R/R)_{strain}$ at $H = 0$ T for the LPCMO(001) film increases with decreasing temperature and reaches a maximal value of 98.6% at $T = 120$ K, indicating the extreme sensitivity of the

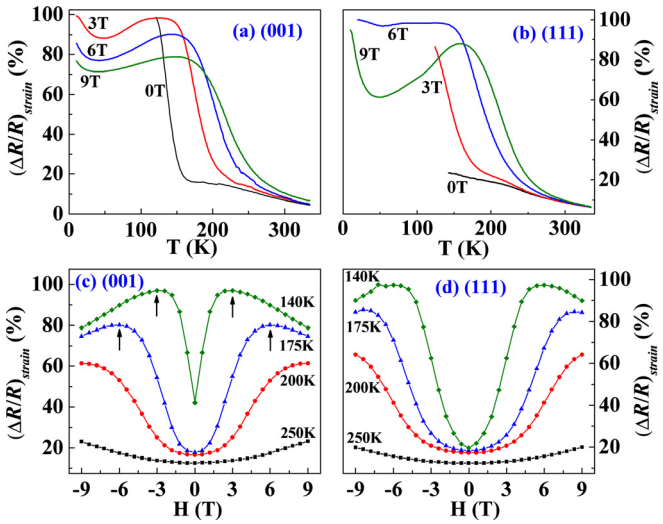

FIG. 4. (a) and (b) show temperature dependence of $(\Delta R/R)_{strain}$ at $H = 0$, 3, 6, and 9 T for the LPCMO films. (c) and (d) show $(\Delta R/R)_{strain}$ versus H curves for the LPCMO films at temperatures as stated.

CO/AFI phase to the lattice strain at low temperatures. It is surprising that the application of a magnetic field strongly influences $(\Delta R/R)_{strain}$. $(\Delta R/R)_{strain}$ is significantly enhanced in high temperature region ($T > 190$ K) and suppressed in low temperature region ($T < 190$ K) by a magnetic field, showing opposing effects of the magnetic field on the strain effect. For example, $(\Delta R/R)_{strain}$ at $T = 200$ K is enhanced from 15% for $H = 0$ T to 65% for $H = 9$ T, an increase of approximately 3.3 times, while $(\Delta R/R)_{strain}$ at $T = 10$ K is reduced from 99.98% for $H = 3$ T to 76.6% for $H = 9$ T. Similar opposing effects of the magnetic field on the strain effect were also observed in the LPCMO(111) film. For example, $(\Delta R/R)_{strain}$ at $T = 160$ K was increased by roughly 3 times under $H = 9T$. Such substantial magnetic-field-induced enhancement of $(\Delta R/R)_{strain}$ has not yet been reported for $R_{1-x}A_xMnO_3$/PMN-PT (R = La, Pr; A = Ca, Sr, Ba) systems.[17,19,22,25–27] These data together tell us that $(\Delta R/R)_{strain}$ or the strain effect is deeply associated with EPS and the larger the relative strength of the EPS, the larger the $(\Delta R/R)_{strain}$. Based on this, it is understandable that the magnetically tunable $(\Delta R/R)_{strain}$ is microscopically a result of the magnetic-field-induced change in the relative strength of the EPS.

To gain insight into the evolution of the relative strength of EPS with magnetic field, we measured $(\Delta R/R)_{strain}$ as a function of H. The results are shown in Figs. 4(c) and 4(d). For the LPCMO(001) film, at a fixed high temperature (e.g., $T = 200$ or 250 K), $(\Delta R/R)_{strain}$ increases monotonously with increasing H, reflecting that the relatively strength of EPS was enhanced continuously by H. However, at a low temperature, e.g., $T = 140$ K, $(\Delta R/R)_{strain}$ initially increases sharply with increasing H and reaches the maximal value at $H = 3$ T, before dropping with further increase in H. This evolution of $(\Delta R/R)_{strain}$ with H implies that the EPS is at its strongest at $H = 3$ T for $T = 140$ K but suppressed when H deviates from $H = 3$ T. For $H < 3$ T, the CO/AFI phase dominates over the FMM phase, while for $H > 3$ T, the latter dominates over the former. At around $H = 3$ T, the film shows the maximal EPS tendency while the energy difference between the coexisting CO/AFI and FMM phases is minimum. A small external perturbation (e.g., the strain) would easily covert the CO/AFI phase into the FMM phase, causing a huge decrease in resistance of up to 97.5%. We note that at $T = 175$ K, the strongest EPS appears at $H = 6$ T, as reflected by the largest $(\Delta R/R)_{strain} \sim 80.1\%$ at $H = 6$ T. Similar effects of magnetic field on $(\Delta R/R)_{strain}$ were also observed for the LPCMO(111) film [Fig. 4(d)].

The poling-induced strain does not only affect the electronic transport properties but also result in magnetization and magnetoresistance changes in the LPCMO(001) and LPCMO(111) films. Similar to findings reported from earlier studies on $La_{1-x-y}Pr_yCa_xMnO_3$ films,[18,28] a pronounced magnetic irreversibility is observed at $T_{CG} \sim 77$ and 53 K between the zero-field-cooled (ZFC) and field-cooled (FC) curves for $H = 200$ and 500 Oe [inset of Fig. 5], respectively. The temperature dependence of FC magnetization of the LPCMO(111) film for the P_r^0 and P_r^+ states are shown in Fig. 5. There was a remarkable increase in the magnetization after the PIN-PMN-PT was poled to the P_r^+ state. The relative change in the in-plane magnetization $\Delta M/M$, $(\Delta M/M = (M(P_r^+) - M(P_r^0)/M(P_r^0))$, reaches 17.4% at $T = 10$ K for $H = 50$ Oe. This result is consistent with the poling-induced conversion of the CO/AFI phase into the FMM phase. We found that associated with these changes in the resistance and magnetization, the magnetoresistance (MR) of the film was also modified significantly by the induced strain. As can be seen in Figs. S2(a) and S2(b) (see supplementary material[24]) MR of both films are enhanced over the entire temperature range after poling. For $H = 3$ T, MR is enhanced by ~30% at $T = 170$ K for the LPCMO(001) film. Generally, the poling-induced maximal change in MR (i.e., ΔMR) decreases with increasing H for both films, as can be seen in the insets of Figs. S2(a) and S2(b),[24] respectively. This is consistent with our earlier discussion that the maximal EPS appears at $H = 3$ T and decreases with increasing H from 3 to 9 T. Such remarkable effects of poling-induced-strain on MR are evident in Figs. S2(c) and S2(d),[24] where MR was plotted against H for the P_r^0 and P_r^+ states,

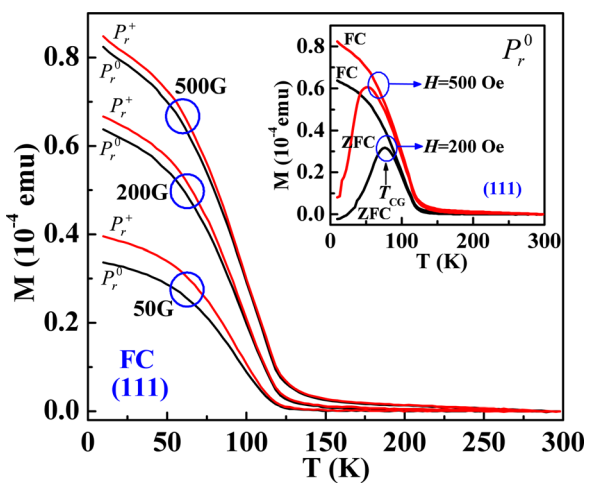

FIG. 5. Temperature dependence of FC magnetization for the LPCMO(111) film when the PIN-PMN-PT substrate was in the P_r^0 and P_r^+ states, respectively. Inset shows the temperature dependence of ZFC and FC magnetization for the LPCMO(111) film when the PIN-PMN-PT substrate was in the unpoled P_r^0 state.

respectively. For both films, *MR* at any fixed temperature was significantly enhanced due to the poling-induced strain that converts CO/AFI phase into the FMM phase and thus, strengthens the EPS. All these data clearly establish that the mutual interactions between the strain and the magnetic field are linked by the EPS, which is critically important to understand the observed results.

In summary, phase-separated LPCMO films were grown on (001)- and (111)-oriented ferroelectric substrates. During poling along the [001] or [111] direction, the variation of the resistance tracks the electric-field-induced in-plane strain efficiently, implying strain but not electrostatic charge-mediated mechanism. Ferroelectric poling causes complete melting of the CO/AFI phase associated with a huge drop in resistance by ~99.98% and considerable enhancement in ferromagnetism, T_C and *MR*. Particularly, we observed opposing effects of magnetic field on the strain-tunability of resistance $[(\Delta R/R)_{strain}]$ at high and low temperatures, respectively. This phenomenon and the magnetic-field tunable strain effect are strongly associated with EPS, whose relative strength can be determined by measuring $(\Delta R/R)_{strain}$ under magnetic fields. Our findings provide an approach to gain deeper insights into the evolution dynamics of EPS with magnetic field.

This work was supported by the National Basic Research Program of China (Grant No. 2012CB922003), the NSFC (Grant Nos. 51172259, 51332007, and 11090332), the CAS/SAFEA International Partnership Program for Creative Research Teams, and the PolyU internal grant (Grant No. G-U846).

[1]M. Uehara, S. Mori, C. H. Chen, and S.-W. Cheong, Nature **399**, 560 (1999).
[2]T. Z. Ward, J. D. Budai, Z. Gai, J. Z. Tischler, L. F. Yin, and J. Shen, Nat. Phys. **5**, 885 (2009).
[3]J. Shen, T. Z. Ward, and L. F. Yin, Chin. Phys. B **22**, 017501 (2013).
[4]H. W. Guo, J. H. Noh, S. Dong, P. D. Rack, Z. Gai, X. S. Xu, E. Dagotto, J. Shen, and T. Z. Ward, Nano Lett. **13**, 3749 (2013).
[5]H. Y. Zhai, J. X. Ma, D. T. Gillaspie, X. G. Zhang, T. Z. Ward, E. W. Plummer, and J. Shen, Phys. Rev. Lett. **97**, 167201 (2006).
[6]M. H. Burkhardt, M. A. Hossain, S. Sarkar, Y.-D. Chuang, A. G. C. Gonzalez, A. Doran, A. Scholl, A. T. Young, N. Tahir, Y. J. Choi, S.-W. Cheong, H. A. Dürr, and J. Stöhr, Phys. Rev. Lett. **108**, 237202 (2012).
[7]L. W. Zhang, C. Israel, A. Biswas, R. L. Greene, and A. de Lozanne, Science **298**, 805 (2002).
[8]S. Singh, M. R. Fitzsimmons, H. Jeen, A. Biswas, and M. E. Hawley, Appl. Phys. Lett. **101**, 022404 (2012).
[9]D. Gillaspie, J. X. Ma, H.-Y. Zhai, T. Z. Ward, H. M. Christen, E. W. Plummer, and J. Shen, J. Appl. Phys. **99**, 08S901 (2006).
[10]T. Wu, S. B. Ogale, S. R. Shinde, A. Biswas, T. Polletto, R. L. Greene, T. Venkatesan, and A. J. Millis, J. Appl. Phys. **93**, 5507 (2003).
[11]H. Jeen and A. Biswas, Phys. Rev. B **83**, 064408 (2011).
[12]E. Dagotto, T. Hotta, and A. Moreo, Phys. Rep. **344**, 1 (2001).
[13]A. Moreo, M. Mayr, A. Feiguin, S. Yunoki, and E. Dagotto, Phys. Rev. Lett. **84**, 5568 (2000).
[14]D. N. Argyriou, U. Ruett, C. P. Adams, J. W. Lynn, and J. F. Mitchell, New J. Phys. **6**, 195 (2004).
[15]P. G. Radaelli, R. M. Ibberson, D. N. Argyriou, H. Casalta, K. H. Andersen, S.-W. Cheong, and J. F. Mitchell, Phys. Rev. B **63**, 172419 (2001).
[16]Y. H. Sun, Y. G. Zhao, H. F. Tian, C. M. Xiong, B. T. Xie, M. H. Zhu, S. Park, W. D. Wu, J. Q. Li, and Q. Li, Phys. Rev. B **78**, 024412 (2008).
[17]M. C. Dekker, A. D. Rata, K. Boldyreva, S. Oswald, L. Schultz, and K. Dorr, Phys. Rev. B **80**, 144402 (2009).
[18]T. Zhang, Q. Wei, R. K. Zheng, X. P. Wang, and Q. F. Fang, J. Appl. Phys. **113**, 013705 (2013).
[19]J. F. Wang, Y. C. Jiang, Z. P. Wu, and J. Gao, Appl. Phys. Lett. **102**, 071913 (2013).
[20]Q. P. Chen, J. J. Yang, Y. G. Zhao, S. Zhang, J. W. Wang, M. H. Zhu, Y. Yu, X. Z. Zhang, Z. Wang, B. Yang, D. Xie, and T. L. Ren, Appl. Phys. Lett. **98**, 172507 (2011).
[21]Y. Y. Zhang, X. B. Li, D. A. Liu, Q. H. Zhang, W. Wang, B. Ren, D. Lin, X. Y. Zhao, and H. S. Luo, J. Cryst. Growth **318**, 890 (2011).
[22]Q. X. Zhu, W. Wang, S. W. Yang, X. M. Li, Y. Wang, H.-U. Habermeier, H. S. Luo, H. L. W. Chan, X. G. Li, and R. K. Zheng, Appl. Phys. Lett. **101**, 172906 (2012).
[23]A. P. Ramirez, P. Schiffer, S.-W. Cheong, C. H. Chen, W. Bao, T. T. M. Palstra, P. L. Gammel, D. J. Bishop, and B. Zegarski, Phys. Rev. Lett. **76**, 3188 (1996).
[24]See supplementary material at http://dx.doi.org/10.1063/1.4860415 for Figs. S1 and S2.
[25]R. B. Gangineni, L. Schultz, C. Thiele, I. Mönch, and K. Dörr, Appl. Phys. Lett. **91**, 122512 (2007).
[26]R. K. Zheng, Y. Wang, Y. K. Liu, G. Y. Gao, L. F. Fei, Y. Jiang, H. L. W. Chan, X. M. Li, H. S. Luo, and X. G. Li, Mater. Chem. Phys. **133**, 42 (2012).
[27]Q. X. Zhu, M. Zheng, M. M. Yang, X. M. Li, Y. Wang, X. Shi, H. L. W. Chan, H. S. Luo, X. G. Li, and R. K. Zheng, Appl. Phys. Lett. **103**, 132910 (2013).
[28]N. S. Bingham, P. Lampen, M. H. Phan, T. D. Hoang, H. D. Chinh, C. L. Zhang, S. W. Cheong, and H. Srikanth, Phys. Rev. B **86**, 064420 (2012).